A Versatile Approach to Electrochemical *in-situ* Ambient Pressure X-ray Photoelectron Spectroscopy: Application to a Complex Model Catalyst

Olaf Brummel,[a,] Yaroslava Lykhach,[a,†,*] Maryline Ralaiarisoa,[b] Matias Berasategui,[b] Maximilian Kastenmeier,[a] Lukáš Fusek,[a,c] Alexander Simanenko,[a] Wenqing Gu,[b] Pip C. J. Clark,[b] Rossella Yivlialin,[b,‡] Michael J. Sear,[b] Josef Mysliveček,[c] Marco Favaro,[b] David E. Starr,[b] Jörg Libuda[a].*

[a]Interface Research and Catalysis, ECRC, Friedrich-Alexander-Universität Erlangen-Nürnberg, Egerlandstrasse 3, 91058 Erlangen, Germany

[b]Helmholtz Zentrum Berlin für Materialien und Energie GmbH, Institute for Solar Fuels, Hahn-Meitner-Platz 1, 14109 Berlin, Germany

[c]Charles University, Faculty of Mathematics and Physics, Department of Surface and Plasma Science, V Holešovičkách 2, 18000 Prague, Czech Republic

Corresponding Authors

*olaf.brummel@fau.de; *yaroslava.lykhach@fau.de

Abstract

We present a new technique for investigating complex model electrocatalysts by means of electrochemical *in-situ* ambient pressure X-ray photoelectron spectroscopy (AP-XPS). Using a specially designed miniature capillary device, we prepared a three-electrode electrochemical cell in a thin layer configuration and analyzed the active electrode/electrolyte interface by using tender X-ray synchrotron radiation. We demonstrate the potential of this versatile method by investigating a complex model electrocatalyst. Specifically, we monitored the oxidation state of Pd nanoparticles supported on an ordered $Co_3O_4(111)$ film on Ir(100) in an alkaline electrolyte under potential control. We found that the Pd oxide formed in the *in-situ* experiment differs drastically from the one observed in an *ex-situ* emersion experiment at similar potential. We attribute these differences to the decomposition of a labile palladium oxide/hydroxide species after emersion. Our experiment demonstrates the potential of our approach and the importance of electrochemical *in-situ* AP-XPS for studying complex electrocatalytic interfaces.

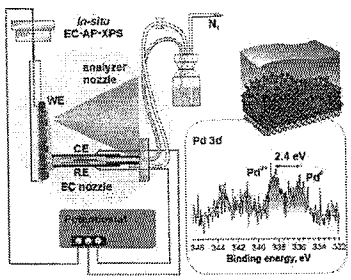

KEYWORDS electrochemical cell for *in-situ* AP-XPS;.palladium; supported nanoparticles; model electrocatalysis; liquid/solid interface.

One of the most powerful approaches to explore complex electrocatalytic materials is the use of well-defined model catalysts, which are studied in liquid electrolytes by *in-situ* methods.[1-5] For example, we recently investigated various types of nanostructured metal/oxide catalysts prepared by surface science methods in ultrahigh vacuum conditions, after transfer to liquid electrolytes under potential control.[6-10] To analyze the oxidation state of such electrocatalysts, photoelectron spectroscopy is a suitable tool, and can be either laboratory-based (XPS) or synchrotron-based (SRPES).[11-15] In the standard approach, these techniques are coupled to an *ex-situ* emersion electrochemical cell. Such *ex-situ* experiments provide information on the oxidation state of the catalyst[16, 17] and the composition of the electric double layer[18] as a function of electrode potential. However, *ex-situ* emersion methods have disadvantages including the potential decomposition of active states after removal from the electrolyte. Therefore, *in-situ* experiments are highly desirable, despite *in-situ* XPS/SRPES in liquid electrolytes and under potential control being a very challenging task. Generally, such studies require stabilization of a liquid electrolyte film that is thin enough to be penetrated by photoelectrons emitted from the liquid/solid interface but thicker than the Debye screening length to be considered a bulk electrolyte.[12, 13] In this respect, tender ($2.0 < h\nu < 7.0$ keV) and hard X-ray ($h\nu > 7.0$ keV) radiation from synchrotron sources is a suitable choice due to the high kinetic energies and, therefore, high inelastic mean free path of the emitted photoelectrons (7.0-20.0 nm).[11-13,19] For instance, the minimum thickness of liquid electrolyte films with the ionic strength of 0.1 M is on the order of tens of nanometers, which requires kinetic energies of photoelectrons emitted from the liquid/solid interface higher than 2500 eV.[19]

Previously, *in-situ* studies of electrified liquid/solid interfaces were realized in several experimental configurations including 'dip and pull',[11-13] 'tilted sample',[20] and 'offset droplet'.[21]

A conceptually different approach employs a membrane-based electrode assembly.[22-24] However, this technique requires the catalytic materials to be deposited directly onto the membrane and, therefore, is not compatible with the use of single crystalline substrates. Among the available methods, the 'dip and pull' technique is the most frequently employed approach for characterizing electrified liquid/solid interfaces of planar samples with ambient pressure XPS (AP-XPS).[11-13, 25, 26] Nevertheless, the method comes with a critical boundary condition. To prepare the liquid film and bring it in front of the electron analyzer, relatively large samples are required, typically with the size of several centimeters. In practice, this turns out to be a great challenge when combining the method with standard surface science experiments, where typical sample sizes are 10 mm or less. Often, it is very difficult (or even impossible) to prepare and characterize single crystalline samples with a size suitable for a conventional 'dip and pull' experiment.

In the current letter, we describe a versatile setup for electrochemical *in-situ* AP-XPS, which is compatible with regularly sized single crystal substrates (10 mm or less). We summarize the concept in Figure 1 and provide the technical details in the Supporting Information, Figures S1-S3. The single crystal-based sample is placed on a specially designed sample holder in front of the analyzer nozzle. The electrochemical cell is a small capillary made of a thermoplastic polymer (polyether ether ketone, PEEK) mounted at the tip of a hollow metallic rod positioned on an X-Y stage and equipped with Z-shift. The sample is the working electrode (WE), while the reference (RE) and counter (CE) electrodes are Pt strips inserted into the channels of the electrochemical cell. The cell is filled with electrolyte through a perfluoroalkoxy alkane (PFA) polymer tube inserted into the supporting hollow stainless steel rod and is connected with the

electrolyte reservoir via the liquid feedthrough. The pressure in the analysis chamber and electrolyte reservoir is equalized by means of a feedback loop made of a PFA tube.

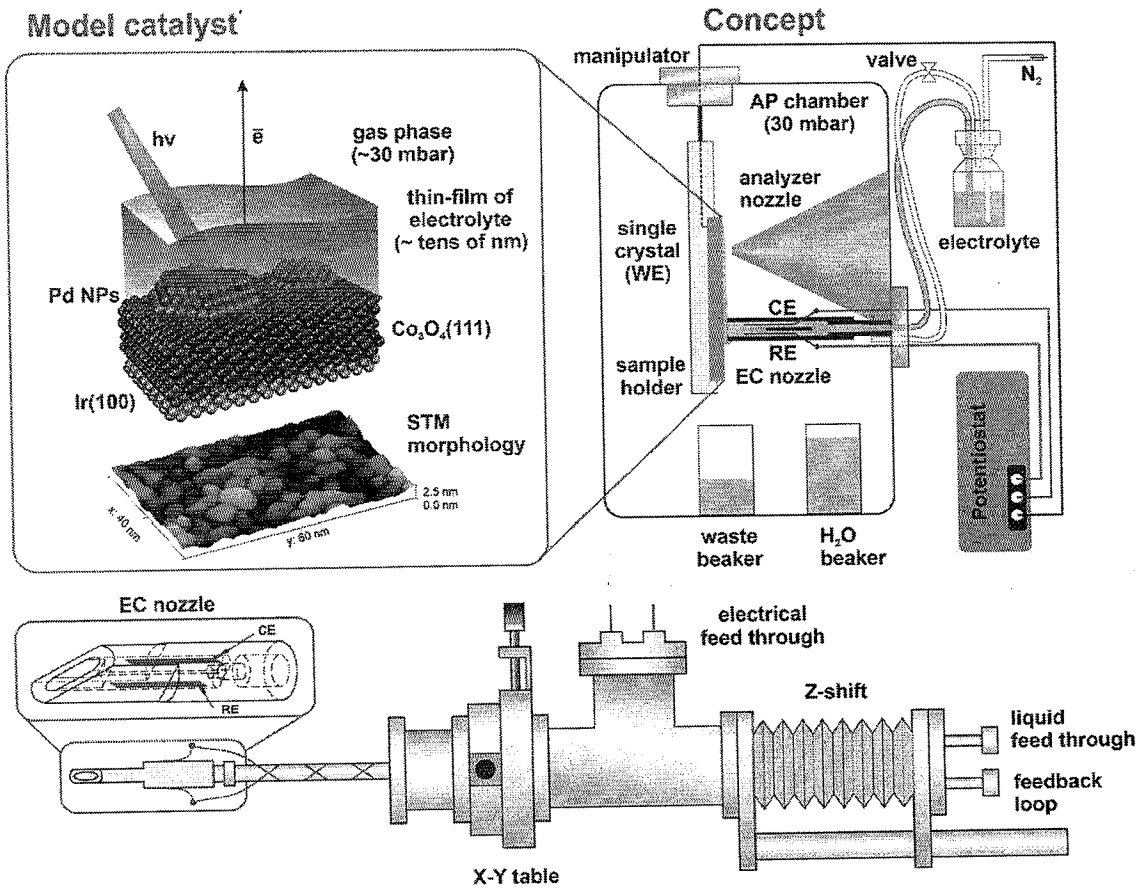

Figure 1. Schematic representation of the new electrochemical *in-situ* AP-XPS cell designed for small single crystal-based samples (top). Setup of the electrochemical cell (bottom).

The electrolyte flow is driven by slight overpressure created in the electrolyte reservoir with N_2 gas while keeping the feedback connection to the analysis chamber closed. The equilibrium between liquid and gas phases was achieved in the analysis chamber at 30 mbar. This pressure was established by the water vapor from a beaker of ultrapure water (~ 50 mL) placed in the analysis chamber and N_2 gas. During the measurements, the WE (i.e. the sample) and the

electron spectrometer were commonly grounded. To ensure that the analyzed part of the sample was in contact with the electrolyte, the following procedure was performed. First, the sample was brought into contact with a standing electrolyte droplet at the end of the capillary; second, from this position the sample was raised to drag the electrolyte to form a thin liquid film without breaking potential control (similar to the 'dip and pull' technique). During this procedure, the distance between the sample and capillary was monitored visually by means of the viewports and a camera. The electrochemical *in-situ* AP-XPS study was performed in a thin film configuration in a static meniscus mode (no electrolyte flow) (Figure 1). The thin electrolyte layer was stable and conductive on the timescale of the experiment (more than 3 hours, see Supporting Information, Figures S4-S5). Some droplets of electrolyte, which occasionally drip down from the sample, were collected in a waste electrolyte beaker placed in the analysis chamber beneath the WE.

In comparison to the conventional 'dip and pull' technique, our setup comes with important advantages: Firstly, the electrochemical cell is placed close to the nozzle of the analyzer (few millimeters), allowing the use of relatively small samples (< 10 mm). Secondly, in the present configuration, both the RE and CE are close to the surface of the WE which may potentially reduce the Ohmic drop. Thirdly, the setup is a bolt-on device that can be used in most AP-XPS systems.

For the experiment described below, the setup was installed at the SpAnTeX end-station served by the KMC-1 beamline of the BESSY II synchrotron facility, Berlin, Germany. The technical details of the SpAnTeX end-station and the specifications of KMC-1 beamline can be found elsewhere.[12, 27]

To demonstrate the potential of our approach, we investigated a $Pd/Co_3O_4(111)$ model electrocatalyst prepared on a Ir(100) single crystal. The choice of the model electrocatalyst was motivated by the superior performance of Pd-based catalysts for ethanol electro-oxidation in alkaline environments.[28] The sample, a disc 10 mm in diameter, was prepared by means of UHV-based surface science methods (see Supporting Information). Previously, we characterized the $Pd/Co_3O_4(111)$ model catalyst with respect to its morphology and the oxidation state of Pd nanoparticles and the $Co_3O_4(111)$ support.[17, 29] Briefly, the $Pd/Co_3O_4(111)$ model catalyst consists of two-dimensional Pd nanoparticles with an average height of 3 ML and a mean diameter of 5.8 nm (see Figure 1) supported on a 6.0 nm thick ordered $Co_3O_4(111)$ film. In UHV, the Pd nanoparticles are predominantly metallic. However, electronic metal support interaction (EMSI) gives rise to the formation of partially oxidized $Pd^{\delta+}$ species at the $Pd/Co_3O_4(111)$ interface and small amounts of atomically dispersed Pd^{2+} species dispersed in $Co_3O_4(111)$.[17]

In the AP-XPS experiment, the sample was brought into contact with the alkaline electrolyte (0.1 M KOH, pH = 13) at defined potentials (see Supporting Information and Figure S6 for experimental details and calibration of potentials). In Figure 2, we show core level spectra of the Pd 3d, O 1s, K 2p, and C 1s obtained from the $Pd/Co_3O_4(111)$ model catalyst under different experimental conditions with a photon energy of 3000 eV. The bottom spectra in Figures 2a-c were obtained from a $Pd/Co_3O_4(111)$ model catalyst under 30 mbar H_2O (hydrated conditions) before contact with the liquid electrolyte. Two contributions were detected in the Pd 3d spectra at 335.9 eV (Pd $3d_{5/2}$) and 338.2 eV (Pd $3d_{5/2}$) associated with metallic Pd^0 and the Pd^{2+} species dispersed in the $Co_3O_4(111)$ substrate, respectively.[17, 29] Unfortunately, we could not identify the contribution from the partially oxidized $Pd^{\delta+}$ species at the Pd/Co_3O_4 interface due to their

relatively low intensity and a high noise-to-signal ratio in the Pd 3d spectra. It should be noted, however, that the binding energy of metallic Pd^0 contribution is higher with respect to the value observed in similar systems in UHV (335.1 eV).[29] The corresponding discrepancy is due to the formation of an adsorbate layer on the surface of the Pd nanoparticles under exposure to 30 mbar H_2O. Typically, the adsorbate induced shifts of the Pd 3d core level are in the range of 0.3-0.6 eV and depend on the nature and the adsorption site of the adsorptive.[30]

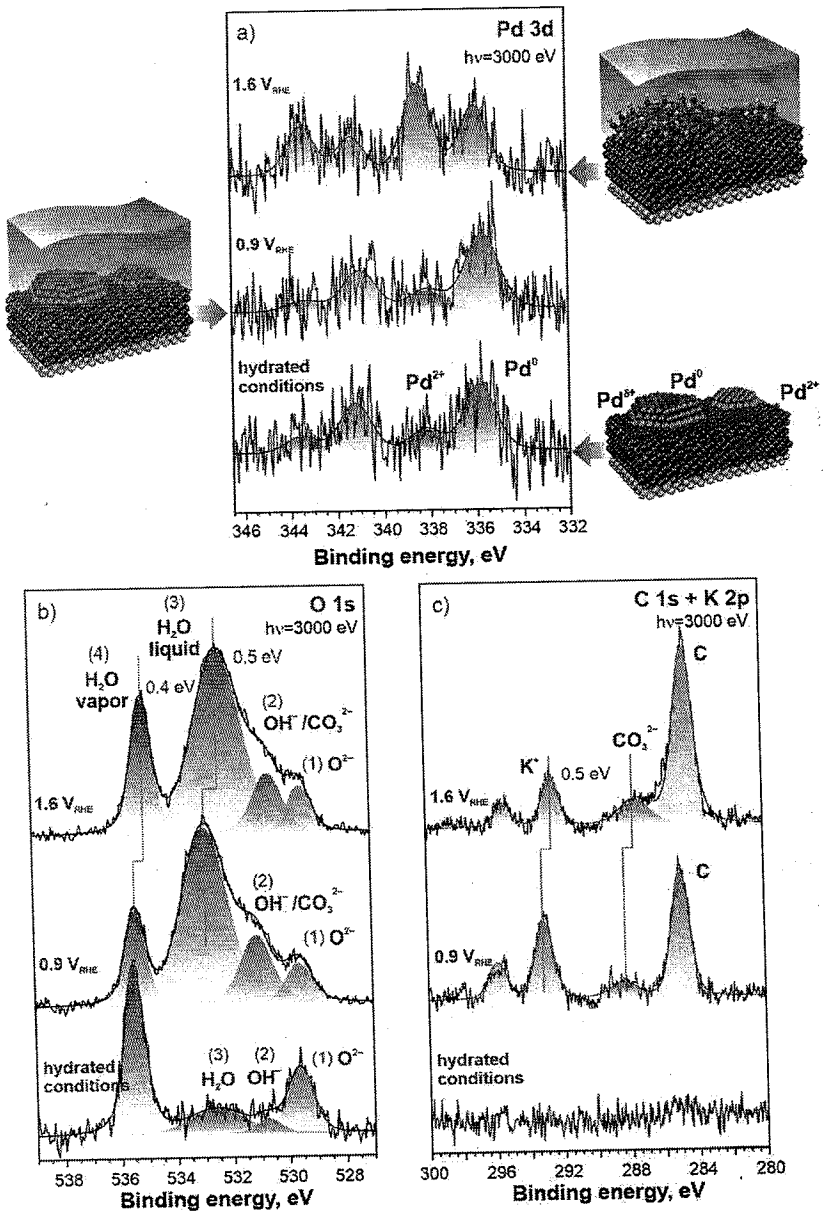

Figure 2. Pd 3d (a), O 1s (b), C 1s and K 2p (c) core level spectra obtained from the $Pd/Co_3O_4(111)$ model catalyst exposed to 30 mbar H_2O (hydrated conditions, bottom spectra) and covered by a thin liquid film of 0.1 M KOH electrolyte under potential control at 0.9 V_{RHE} and 1.6 V_{RHE}. The spectra were acquired with a photon energy of 3000 eV.

Earlier, we observed similar shifts of the Pd 3d core level in the $Pd/Co_3O_4(111)$ system exposed to 1 mbar H_2O.[29]

The four components in the O 1s spectra observed under hydrated conditions are assigned to the contributions from lattice oxygen in the $Co_3O_4(111)$ film (1), OH^- species (2), physisorbed/liquid H_2O (3), and vapor H_2O (4). Note that the contributions (2) and (3) partially overlap with the Pd $3p_{3/2}$ signal which is, however, insignificant under the present conditions. In the combined C 1s and K 2p region, we observed traces of surface carbon only.

In the next step, the spectra were obtained from the $Pd/Co_3O_4(111)$ model catalyst covered by a thin layer of electrolyte at the potentials of 0.9 V_{RHE} and 1.6 V_{RHE}. We found that Pd 3d spectra remain virtually unchanged at 0.9 V_{RHE}. However, upon increasing the potential to 1.6 V_{RHE}, we observed the emergence of a new contribution at 338.4 eV which is slightly shifted to higher binding energies with respect to the one earlier assigned to the Pd^{2+} species dispersed on $Co_3O_4(111)$ (338.2 eV). Unfortunately, we could not reliably resolve the two contributions due to large noise in the Pd 3d spectra. Most importantly, the emergence of the contribution at 338.4 eV indicates strong oxidation of supported Pd nanoparticles driven by applied potential. Also, this observation clearly shows that liquid film is conductive and it is possible to control the potential of the model electrode. We discuss the nature of the palladium oxide in more details below.

The formation of the liquid electrolyte layer has a strong influence on the O 1s, C 1s, and K 2p spectra. In particular, we found a strong increase of the contributions (2) and (3) in the O 1s spectra and the emergence of additional contributions from potassium and carbon in the K 2p and C 1s regions. Note that a new contribution at 288.4 eV at 0.9 V_{RHE} is most likely associated with carbonate (CO_3^{2-}) and/or carboxylate species.[31] These species may result from CO_2 and carboxylic acids present in the atmosphere, which are rapidly adsorbed by liquid water

interacting strongly with oxide based materials.[32] The corresponding carbonate/carboxylate contribution in O 1s spectrum was reported at 531.0 eV.[31] Thus, the peak (2) in O 1s spectrum represents a joint contribution from OH^- and carbonates/carboxylates, while the peak (3) solely represents liquid H_2O. Additionally, at 1.6 V_{RHE}, the peak (2) may partially overlap with the O 1s contribution from palladium oxide.[33]

We performed quantitative analysis of the thickness and the ionic strength of the liquid electrolyte film based on the intensities of the peaks (1)-(3) in the O 1s spectra (see Supporting Information, Tables S1 and S3). In the present study, the inelastic mean free path (IMFP) of the photoelectrons with kinetic energy of ~2460 eV passing through a liquid water layer is in the range of 8-9 nm.[19] The thickness of the liquid electrolyte layer, as calculated from the ratio of O 1s contributions (3) and (1), is in the range of 13 nm (see Supporting Information, Table S1). The ionic strength of the electrolyte within the liquid film was analyzed based on the intensity ratio between the O 1s contributions (3) and (2). Surprisingly, we obtained a factor of 3.2 instead of a factor of 555 (expected for pure 0.1 M KOH solution, see Table S2). This discrepancy may appear due to several reasons including (i) non-uniform distribution of ions within the Debye screening length with respect to the bulk electrolyte,[34] (ii) an increased concentration of the electrolyte due to evaporation (possibly also leading to the formation of dry patches at the liquid/solid interface), and (iii) considerable amount of carbonates or carboxylates in the electrolyte. The corresponding estimations based on the intensities of O 1s, C 1s, and K 2p core levels are summarized in Table S3.

We found that non-uniform distribution of ions within the Debye length at the liquid/solid interface cannot explain the observed low intensity ratio. For instance, using a Simulation of Electron Spectra for Surface Analysis tool (SESSA),[35] a simulation of the increase of the ionic

concentration by 60 times (from 0.1 M KOH to 6.0 M KOH) within a thickness equivalent to three Debye lengths at the solid/liquid interface (2.88 nm, Debye length is 0.96 nm for 0.1 M KOH) in liquid film with a total thickness of 13 nm yielded the intensity ratio of 97 ~~(data not shown)~~. It is more likely that the concentration of the electrolyte increases due to partial evaporation of water. Regarding the continuity of electrolyte film, we also cannot completely rule out the existence of the dry patches. The loss of water is corroborated by the finding the contribution from K 2p accounts for about 30% of the intensity of the O 1s contribution (2). This corresponds to the ionic strength of about 9 M KOH. Generally, this finding is in line with a strong enrichment of the supporting electrolyte in the thin film. We propose that the strongly increased ionic strength is an important mechanism that stabilizes the liquid film on the surface against evaporation. The hygroscopic nature of the concentrated KOH solution will stabilize the electrolyte film when the partial pressure of water in the chamber deviates from the vapor pressure. Finally, if we assume that the C 1s peak at 288.4 eV solely represents carbonates, the corresponding contribution in O 1s spectrum would constitute nearly 100% of the intensity of peak (2). If the main reason for the high intensity of O 1s contribution (2) would be the presence of carbonates, this carbonate-rich electrolyte would have a similar stabilizing effect on the liquid electrolyte film.

Importantly, we found that the binding energy positions of the contributions (2) and (3) associated with OH^-/CO_3^{2-}/carboxylates and H_2O in the O 1s region and the contributions from potassium ions and CO_3^{2-}/carboxylate species in the K 2p and C 1s regions shift consistently to lower binding energies when switching the potential from 0.9 to 1.6 V_{RHE}. This observation confirms that the liquid film is electrically conductive. The observed shift is 0.5 eV, which is slightly lower than the potential difference of 0.7 V_{RHE} applied in the experiment. It was reported

earlier that the shift of the core levels per applied potential should be 1 eV/V.[11] There are several reasons that could contribute to the deviation from this value. First, we probe through a gradient of the local potentials perpendicular to the surface plane, due to the Helmholtz layer formed at the interface. Second, we may consider significant Ohmic drops in the thin film along the axis parallel to the surface plane. Third, we expect some variation of the true potential over time caused by the use of a quasi-reference electrode and long measuring times on the order of hours. Finally, we assume that the thickness of the liquid film may change locally and dynamically, directly affecting the first and second point. All of these factors may lead to a broadening of the signal and a reduced binding energy shift. Additionally, we found that the contribution (4) associated with the H_2O vapor shifts by about 0.4 eV to lower binding energies, which is also smaller than the difference of potentials. This observation is, however, in line with the fact that the gas phase signal is averaged over the region between the electrolyte surface and the electron analyzer. In contrast, the binding energies of the Pd 3d contributions are not influenced by the applied potential due to a common ground between the sample and the analyzer (as noted above).

Finally, we discuss the nature of palladium oxide formed under *in-situ* electrochemical conditions (in-situ EC-AP-XPS) with respect to the *ex-situ* emersion experiment (ex-situ EC-SRPES)[17] and the oxidation experiment under 1 mbar O_2 (NAP XPS).[29] The $Pd/Co_3O_4(111)$ systems used in these studies were prepared under identical conditions and have similar structure, morphology, and composition. The corresponding spectra are compared in Figure 3b. For comparison, we also show the Pd 3d spectra obtained from the similar samples under more reducing conditions in Figure 3a. The Pd 3d spectra under more reducing conditions reveal predominantly a metallic state of the supported Pd nanoparticles. Note that the spectra shown in Figure 3 were obtained with different photon energies and, accordingly, with different sampling

depth (see caption of Figure 3 and Table S4). This resulted, for instance, in a higher intensity of the contributions associated with $Pd^{\delta+}$ and Pd^{2+} species dispersed on $Co_3O_4(111)$ in the Pd 3d spectra obtained in NAP XPS and *in-situ* EC-AP-XPS, respectively, (Figure 3a). Generally, the structure of the Pd 3d spectra remains unchanged in both the *ex-situ* EC-SRPES and in the *in-situ* EC-AP-XPS experiment at 0.9 V_{RHE}. We note that the potential of 0.9 V_{RHE} falls into a region where the formation of surface oxide on Pd(111) has been reported.[36] The lack of significant change in the Pd 3d spectra, however, rather suggests that the formation of surface hydroxyl groups occurs without a major influence on the oxidation state of Pd. In contrast, formation of palladium oxides give rise to significant shifts of the spectral contributions towards higher binding energies with respect to the metallic state. Noteworthy, the binding energy shift between the contributions from palladium oxide and metallic Pd^0 is much larger for *in-situ* emersion at 1.6 V_{RHE} (2.4 eV) than the value observed after *ex-situ* emersion at 1.5 V_{RHE} (1.4 eV) and after exposure to 1 mbar O_2 at 500 K (1.1 eV) (see Figure 3b). Still, this shift is lower than the value reported for PdO_2 (i.e. 3.0 eV).[37] Regarding the nature of the palladium oxide, we propose that the palladium oxides observed at similar potentials in the *in-situ* EC-AP-XPS experiment at 1.6 V_{RHE} and the *ex-situ* EC-SRPES experiment at 1.5 V_{RHE} differ substantially. We attribute these differences to the formation of labile and highly oxidized palladium oxide species in the *in-situ* EC-AP-XPS experiment at 1.6 V_{RHE}. We assume that these species will spontaneously decompose after removal from the electrolyte and hydrated conditions to more stable state which is similar to this observed in the *ex-situ* EC-SRPES experiment after emersion at 1.5 V_{RHE}. We speculate that the high binding energy shift of the palladium oxide contribution with respect to the metallic state (2.4 eV) may result from the complexation of the Pd cations by negatively charged hydroxyl groups. Earlier, Jeong et al.[33] reported substantial shifts of Pd 3d core levels as

a function of the degree of surface hydroxylation of the palladium oxide under NAP XPS conditions. In particular, the highest binding energy of the Pd 3d contribution was observed at 338.5 eV which is close to this observed in the *in-situ* EC-AP-XPS experiment at 1.6 V_{RHE} (338.4 eV). The corresponding highly hydroxylated/hydrated state of palladium oxide was reported to be stable only under 0.5 mbar H_2O.

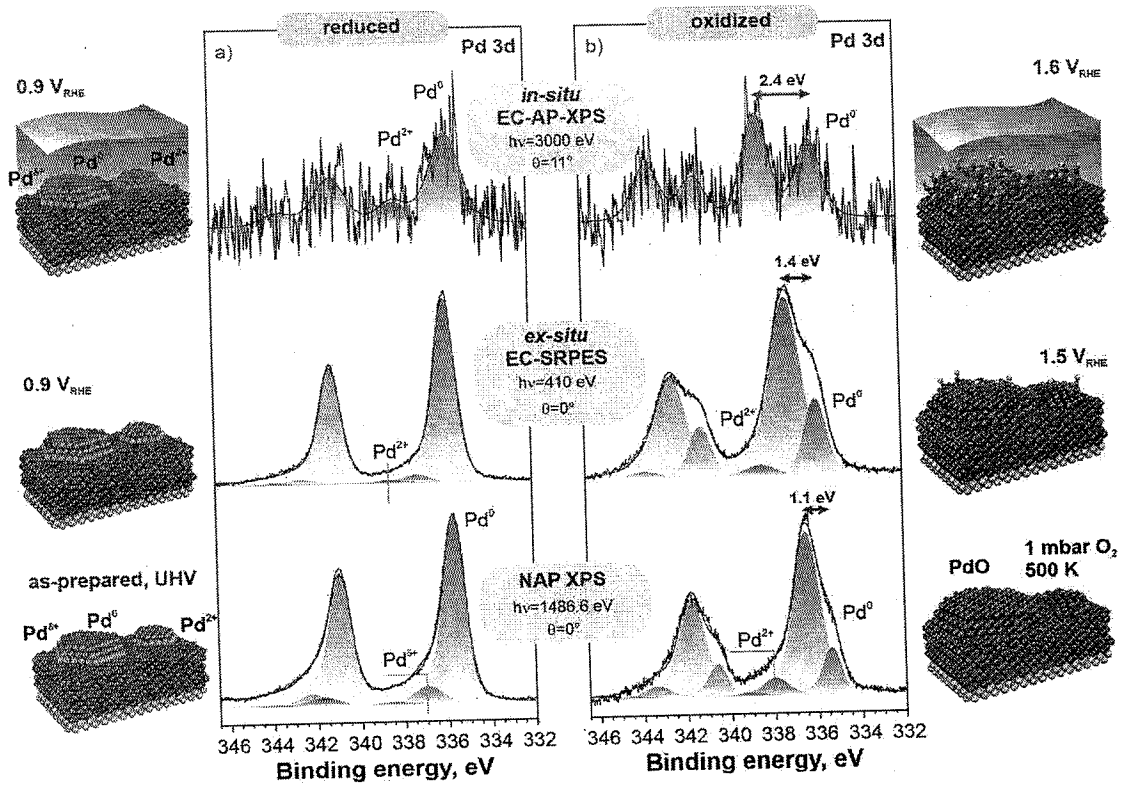

Figure 3. The Pd 3d spectra obtained from the $Pd/Co_3O_4(111)$ model catalyst under reducing (a) and oxidizing (b) conditions established during the NAP XPS (bottom spectra, adapted with permission from Ref. 29. Copyright 2021 American Chemical Society), *ex-situ* emersion EC-SRPES (middle spectra, adapted with permission from Ref. 17. Copyright 2022 American Chemical Society), and electrochemical *in-situ* AP-XPS (top spectra). The spectra were acquired with different photon energies and emission angles θ with respect to surface normal during NAP

XPS (monochromatized Al Kα X-ray source, hν=1486.6 eV, θ=0°), *ex-situ* EC-SRPES (hν=410 eV, θ=0°), and *in-situ* EC-AP-XPS (hν=3000 eV, θ=11°). For detailed interpretation of the spectral contributions from NAP XPS and *ex-situ* EC-SRPES experiments, see Refs. 17, 29.

We found that the total Pd 3d intensity with respect to the O 1s contribution from $Co_3O_4(111)$ increased by as much as 40% at 1.6 V_{RHE} with respect to this at 0.9 V_{RHE}. We rule out any major changes in the morphology of Pd nanoparticles because these would lead to a much stronger variations in the intensities of Pd 3d and O 1s contributions. Instead, we assume that a fraction of Pd^{2+} complexes could be dissolved in the electrolyte and therefore could move closer to the surface of the liquid film. Earlier, we observed a partial dissolution and a loss of about 15% Pd in the *ex-situ* EC-SRPES experiment.[17] The species that are the most prone to dissolution are Pd^{2+} dispersed on $Co_3O_4(111)$ while oxidized Pd nanoparticles are fairly resistant to dissolution into electrolyte.[17] With respect to the reversibility of the oxidation state of supported Pd nanoparticles we refer to our earlier study.[17] Briefly, we found that the oxidation of supported Pd nanoparticles is a reversible process.[17]

It should be noted that we did not observe any clear signs of irradiation damage in our system. Nevertheless, typical mitigation strategies can be employed with our setup, such as a systematic shifting of the sample or refreshing of the thin liquid layer.

In summary, we describe a new and versatile approach to *in-situ* AP-XPS, which is based on a miniature capillary cell. The cell is compatible with typical AP-XPS systems and can be operated in a three-electrode setup in thin film configuration. In contrast to the conventional 'dip and pull' method, our approach is compatible with small single crystal samples (< 10 mm diameter). To demonstrate the potential of our approach, we performed an electrochemical *in-situ* study on a complex model electrocatalyst consisting of Pd nanoparticles supported on an ordered

$Co_3O_4(111)$ film on Ir(100). We show that the surface Pd species observed in the *in-situ* experiment at oxidizing potential (1.6 V_{RHE}, pH = 13) differ drastically from those observed under similar conditions in an *ex-situ* emersion experiment. We attribute the difference to the formation of labile Pd oxide/hydroxide species. We assume that these species decompose after emersion and removal from hydrated conditions to more state as observed in the *ex-situ* EC-SRPES experiment. This observation highlights the importance of *in-situ* AP-XPS in the analysis of the active state of complex electrocatalyst. From the experimental point of view, such studies should become much simpler with the here described setup.

ASSOCIATED CONTENT

Supporting Information.

The following files are available free of charge.

Supporting Information.pdf (PDF)

Experimental details, estimations of the thickness and the ionic strength of the electrolyte in the thin film, calibration of potentials, schematics of the setup.

AUTHOR INFORMATION

Notes

† Also first author

‡ Current Address: Politecnico di Milano, Department of Physics, p.zza Leonardo da Vinci 32, 20133 Milan, Italy

The authors declare no competing financial interests.

ACKNOWLEDGMENT

O.B., Y.L., and J.M. acknowledge financial support by the Deutsche Forschungsgemeinschaft (DFG) (project 431733372) and the Czech Science Foundation (project GAČR 20-11688J). Measurements were carried out at the SpAnTeX end-station at KMC-1 beamline at the BESSY II electron storage ring. The end-station operates within the Berlin joint laboratory for ElectroChemical interfaces (BElChem), and was supported by the Helmholtz Association through the Helmholtz Energy Materials Foundry (HEMF, GZ 714-48172-21/1). M.B., R.Y., and M.R. acknowledge the financial support by projects CATLAB (M.B.), UniSysCat (R.Y.), and GEP-KOE (M.R). O.B. and Y.L. thankfully acknowledge the financial support by HZB. Support is acknowledged by the DFG via Collaborative Research Centre SFB 1452 – Catalysis at Liquid Interfaces (project 431791331) and project 453560721. ~~J.L. acknowledges financial support by the Deutsche Forschungsgemeinschaft (DFG) (project 453560721).~~ L.F. thanks for the support of the Grant Agency of the Charles University (project GAUK 262120). We would like to thank the mechanical workshops at Friedrich-Alexander-Universität Erlangen-Nürnberg and Helmholtz Institute for manufacturing the equipment.

REFERENCES

(1) Bian, J.; Wei, C.; Wen, Y.; Zhang, B., Regulation of Electrocatalytic Activity by Local Microstructure: Focusing on the Catalytic Active Zone. *Chem. - Eur. J.* **2022,** *28* (8), e202103141.

(2) Su, X.; Ye, J.; Zhu, Y., Advances in in-situ Characterizations of Electrode Materials for Better Supercapacitors. *Journal of Energy Chemistry* **2021,** *54*, 242-253.

(3) Bandarenka, A. S.; Ventosa, E.; Maljusch, A.; Masa, J.; Schuhmann, W., Techniques and Methodologies in Modern Electrocatalysis: Evaluation of Activity, Selectivity and Stability of Catalytic Materials. *Analyst* **2014,** *139* (6), 1274-1291.

(4) Reikowski, F.; Maroun, F.; Pacheco, I.; Wiegmann, T.; Allongue, P.; Stettner, J.; Magnussen, O. M., Operando Surface X-ray Diffraction Studies of Structurally Defined Co_3O_4 and CoOOH Thin Films during Oxygen Evolution. *ACS Catal.* **2019,** *9* (5), 3811-3821.

(5) Huang, Y.-F.; Kooyman, P. J.; Koper, M. T. M., Intermediate Stages of Electrochemical Oxidation of Single-Crystalline Platinum Revealed by in situ Raman Spectroscopy. *Nat. Commun.* **2016,** *7*, 12440.

(6) Faisal, F.; Stumm, C.; Bertram, M.; Waidhas, F.; Lykhach, Y.; Cherevko, S.; Xiang, F.; Ammon, M.; Vorokhta, M.; Šmíd, B.; Skála, T.; Tsud, N.; Neitzel, A.; Beranová, K.; Prince, K. C.; Geiger, S.; Kasian, O.; Wähler, T.; Schuster, R.; Schneider, M. A.; Matolín, V.; Mayrhofer, K. J. J.; Brummel, O.; Libuda, J., Electrifying Model Catalysts for Understanding Eectrocatalytic Reactions in Liquid Electrolytes. *Nat. Mater.* **2018,** *17*, 592–598.

(7) Faisal, F.; Bertram, M.; Stumm, C.; Waidhas, F.; Brummel, O.; Libuda, J., Preparation of Complex Model Electrocatalysts in Ultra-High Vacuum and Transfer into the Electrolyte for Electrochemical IR Spectroscopy and Other Techniques. *Rev. Sci. Instrum.* **2018,** *89* (11), 114101.

(8) Yang, T.; Kastenmeier, M.; Ronovský, M.; Fusek, L.; Skála, T.; Waidhas, F.; Bertram, M.; Tsud, N.; Matvija, P.; Prince, K. C.; Matolín, V.; Liu, Z.; Johánek, V.; Mysliveček, J.; Lykhach, Y.; Brummel, O.; Libuda, J., Selective Electrooxidation of 2-Propanol on Pt

Nanoparticles Supported on Co_3O_4: An In-situ Study on Atomically Defined Model Systems. *J. Phys. D: Appl. Phys.* **2021,** *54*, 164002.

(9) Brummel, O.; Libuda, J., Electrifying Oxide Model Catalysis: Complex Electrodes Based on Atomically-Defined Oxide Films. *Catal. Lett.* **2020,** *150* (6), 1546-1560.

(10) Stumm, C.; Bertram, M.; Kastenmeier, M.; Speck, F. D.; Sun, Z.; Rodríguez-Fernández, J.; Lauritsen, J. V.; Mayrhofer, K. J. J.; Cherevko, S.; Brummel, O.; Libuda, J., Structural Dynamics of Ultrathin Cobalt Oxide Nanoislands under Potential Control. *Adv. Funct. Mater.* **2021,** *31*, 2009923.

(11) Axnanda, S.; Crumlin, E. J.; Mao, B.; Rani, S.; Chang, R.; Karlsson, P. G.; Edwards, M. O. M.; Lundqvist, M.; Moberg, R.; Ross, P.; Hussain, Z.; Liu, Z., Using "Tender" X-ray Ambient Pressure X-Ray Photoelectron Spectroscopy as A Direct Probe of Solid-Liquid Interface. *Scientific Reports* **2015,** *5*, 9788.

(12) Favaro, M.; Clark, P. C. J.; Sear, M. J.; Johansson, M.; Maehl, S.; van de Krol, R.; Starr, D. E., Spectroscopic Analysis with Tender X-Rays: SpAnTeX, a New AP-HAXPES end-station at BESSY II. *Surf. Sci.* **2021,** *713*, 121903.

(13) Favaro, M.; Abdi, F. F.; Crumlin, E. J.; Liu, Z.; van de Krol, R.; Starr, D. E., Interface Science Using Ambient Pressure Hard X-ray Photoelectron Spectroscopy. *Surfaces* **2019,** *2* (1), 78-99.

(14) Crumlin, E. J.; Liu, Z.; Bluhm, H.; Yang, W.; Guo, J.; Hussain, Z., X-Ray Spectroscopy of Energy Materials under in situ/Operando Conditions. *J. Electron Spectrosc. Relat. Phenom.* **2015,** *200*, 264-273.

(15) Foelske-Schmitz, A., X-Ray Photoelectron Spectroscopy in Electrochemistry Research. In *Encyclopedia of Interfacial Chemistry: Surface Science and Electrochemistry*, Wandelt, K., Ed. Elsevier: 2018; pp 591-606.

(16) Bertram, M.; Prössl, C.; Ronovský, M.; Knöppel, J.; Matvija, P.; Fusek, L.; Skála, T.; Tsud, N.; Kastenmeier, M.; Matolín, V.; Mayrhofer, K. J. J.; Johánek, V.; Mysliveček, J.; Cherevko, S.; Lykhach, Y.; Brummel, O.; Libuda, J., Cobalt Oxide-Supported Pt Electrocatalysts: Intimate Correlation between Particle Size, Electronic Metal Support Interaction and Stability. *J. Phys. Chem. Lett.* **2020,** *11* (9), 8365–8371.

(17) Kastenmeier, M.; Fusek, L.; Deng, X.; Skála, T.; Mehl, S.; Tsud, N.; Grau, S.; Stumm, C.; Uvarov, V.; Johánek, V.; Libuda, J.; Lykhach, Y.; Mysliveček, J.; Brummel, O., Particle Size and Shape Effects in Electrochemical Environments: Pd Particles Supported on Ordered Co_3O_4(111) and Highly Oriented Pyrolytic Graphite. *J. Phys. Chem. C* **2022,** *126* (30), 12870–12881.

(18) Hansen, W. N.; Kolb, D. M.; Rath, D. L.; Wille, R., An ESCA Study on Emersed Electrodes. *J. Electroanal. Chem. Interfacial Electrochem.* **1980,** *110* (1), 369-373.

(19) Karslıoğlu, O.; Nemšák, S.; Zegkinoglou, I.; Shavorskiy, A.; Hartl, M.; Salmassi, F.; Gullikson, E. M.; Ng, M. L.; Rameshan, C.; Rude, B.; Bianculli, D.; Cordones, A. A.; Axnanda, S.; Crumlin, E. J.; Ross, P. N.; Schneider, C. M.; Hussain, Z.; Liu, Z.; Fadley, C. S.; Bluhm, H., Aqueous Solution/Metal Interfaces Investigated in Operando by Photoelectron Spectroscopy. *Faraday Discuss.* **2015,** *180* (0), 35-53.

(20) Weingarth, D.; Foelske-Schmitz, A.; Wokaun, A.; Kötz, R., In situ Electrochemical XPS Study of the Pt/[EMIM][BF4] System. *Electrochem. Commun.* **2011,** *13* (6), 619-622.

(21) Booth, S. G.; Tripathi, A. M.; Strashnov, I.; Dryfe, R. A. W.; Walton, A. S., The Offset Droplet: a New Methodology for Studying the Solid/Water Interface Using X-Ray Photoelectron Spectroscopy. *J. Phys.: Condens. Matter* **2017,** *29* (45), 454001.

(22) Streibel, V.; Hävecker, M.; Yi, Y.; Velasco Vélez, J. J.; Skorupska, K.; Stotz, E.; Knop-Gericke, A.; Schlögl, R.; Arrigo, R., In Situ Electrochemical Cells to Study the Oxygen Evolution Reaction by Near Ambient Pressure X-ray Photoelectron Spectroscopy. *Top. Catal.* **2018,** *61* (20), 2064-2084.

(23) Velasco-Velez, J. J.; Pfeifer, V.; Hävecker, M.; Weatherup, R. S.; Arrigo, R.; Chuang, C.-H.; Stotz, E.; Weinberg, G.; Salmeron, M.; Schlögl, R.; Knop-Gericke, A., Photoelectron Spectroscopy at the Graphene–Liquid Interface Reveals the Electronic Structure of an Electrodeposited Cobalt/Graphene Electrocatalyst. *Angew. Chem., Int. Ed.* **2015,** *54* (48), 14554-14558.

(24) Law, Y. T.; Zafeiratos, S.; Neophytides, S. G.; Orfanidi, A.; Costa, D.; Dintzer, T.; Arrigo, R.; Knop-Gericke, A.; Schlögl, R.; Savinova, E. R., In situ Investigation of Dissociation and Migration Phenomena at the Pt/Electrolyte Interface of an Electrochemical Cell. *Chem. Sci.* **2015,** *6* (10), 5635-5642.

(25) Favaro, M.; Valero-Vidal, C.; Eichhorn, J.; Toma, F. M.; Ross, P. N.; Yano, J.; Liu, Z.; Crumlin, E. J., Elucidating the Alkaline Oxygen Evolution Reaction Mechanism on Platinum. *J. Mater. Chem. A* **2017,** *5* (23), 11634-11643.

(26) Stoerzinger, K. A.; Favaro, M.; Ross, P. N.; Yano, J.; Liu, Z.; Hussain, Z.; Crumlin, E. J., Probing the Surface of Platinum during the Hydrogen Evolution Reaction in Alkaline Electrolyte. *J. Phys. Chem. B* **2018,** *122* (2), 864-870.

(27) Schaefers, F.; Mertin, M.; Gorgoi, M., KMC-1: A High Resolution and High Flux Soft X-Ray Beamline at BESSY. *Rev. Sci. Instrum.* **2007,** *78* (12), 123102.

(28) Monyoncho, E. A.; Woo, T. K.; Baranova, E. A., Ethanol Electrooxidation Reaction in Alkaline Media for Direct Ethanol Fuel Cells. In *Electrochemistry*, The Royal Society of Chemistry: 2019; Vol. 15, pp 1-57.

(29) Schuschke, C.; Fusek, L.; Uvarov, V.; Vorokhta, M.; Šmíd, B.; Johánek, V.; Lykhach, Y.; Libuda, J.; Mysliveček, J.; Brummel, O., Stability of the Pd/Co_3O_4(111) Model Catalysts in Oxidizing and Humid Environments. *J. Phys. Chem. C* **2021,** *125* (5), 2907–2917.

(30) Nilsson, V.; Van den Bossche, M.; Hellman, A.; Grönbeck, H., Trends in Adsorbate Induced Core Level Shifts. *Surf. Sci.* **2015,** *640*, 59-64.

(31) Ferstl, P.; Mehl, S.; Arman, M. A.; Schuler, M.; Toghan, A.; Laszlo, B.; Lykhach, Y.; Brummel, O.; Lundgren, E.; Knudsen, J.; Hammer, L.; Schneider, M. A.; Libuda, J., Adsorption and Activation of CO on Co_3O_4(111) Thin Films. *J. Phys. Chem. C* **2015,** *119* (29), 16688-16699.

(32) Balajka, J.; Hines, M. A.; DeBenedetti, W. J. I.; Komora, M.; Pavelec, J.; Schmid, M.; Diebold, U., High-Affinity Adsorption Leads to Molecularly Ordered Interfaces on TiO_2 in Air and Solution. *Science* **2018,** *361* (6404), 786-789.

(33) Jeong, B.; Lee, D.; Park, J.-I.; Lee, S. M., Near Ambient Pressure XPS Investigation of Hydrous Palladium Oxide under Water and Oxygen Gas Environments. *J. Phys. D: Appl. Phys.* **2021,** *54* (32), 324001.

(34) Xue, S.; Garlyyev, B.; Auer, A.; Kunze-Liebhäuser, J.; Bandarenka, A. S., How the Nature of the Alkali Metal Cations Influences the Double-Layer Capacitance of Cu, Au, and Pt Single-Crystal Electrodes. *J. Phys. Chem. C* **2020,** *124* (23), 12442-12447.

(35) Smekal, W.; Werner, W. S. M.; Powell, C. J., Simulation of Electron Spectra for Surface Analysis (SESSA): a Novel Software Tool for Quantitative Auger-Electron Spectroscopy and X-Ray Photoelectron Spectroscopy. *Surf. Interface Anal.* **2005,** *37* (11), 1059-1067.

(36) Grdeń, M.; Łukaszewski, M.; Jerkiewicz, G.; Czerwiński, A., Electrochemical Behaviour of Palladium Electrode: Oxidation, Electrodissolution and Ionic Adsorption. *Electrochim. Acta* **2008,** *53* (26), 7583-7598.

(37) Kibis, L. S.; Stadnichenko, A. I.; Koscheev, S. V.; Zaikovskii, V. I.; Boronin, A. I., Highly Oxidized Palladium Nanoparticles Comprising Pd^{4+} Species: Spectroscopic and Structural Aspects, Thermal Stability, and Reactivity. *J. Phys. Chem. C* **2012,** *116* (36), 19342-19348.